LRP 368/89 June 1989

EFFECT OF POWER REFLECTION ON THE OPERATION OF A LOW Q 8 GHz GYROTRON

P. Muggli, M.Q. Tran, T.M. Tran, H.-G. Mathews,
G. Agosti, S. Alberti and A. Perrenoud

submitted for publication in
IEEE Transactions on Microwave Theory and Techniques

EFFECT OF POWER REFLECTION ON THE OPERATION OF A LOW Q 8 GHz GYROTRON

P. Muggli, M.Q. Tran, T.M. Tran,
H.-G. Mathews*, G. Agosti*, S. Alberti and A. Perrenoud

Centre de Recherches en Physique des Plasmas
Association Euratom - Confédération Suisse
Ecole Polytechnique Fédérale de Lausanne
21, Av. des Bains, CH-1007 Lausanne, Switzerland

*ABB INFOCOM SA, EKR Dept., CH-5401 Baden, Switzerland

Abstract

The operating characteristics of a low Q (Q_{cav}=225), 8 GHz gyrotron oscillator operating in TE^{o}_{011} mode and submitted to various mismatched loads are reported. Under matched conditions, output power up to 310 kW (η=35%) and maximum efficiency up to 43% have been measured. In general, power reflection from loads with different phase and amplitude leads to an output power decrease. Too high reflections cause mode switching (TE^{o}_{011} to TE^{o}_{012}) or even arcing inside the tube. The effect of power reflection is seen to increase rapidly with current and output power. Nevertheless, we have observed that, as predicted by the calculations, the maximum output power is not reached under matched conditions but with a specific value of the complex reflection coefficient.

I. INTRODUCTION

High power CW gyrotrons are presently under development in the frequency range from 8 to 280 GHz [1,2]. Heating and current drive of thermonuclear plasmas require tube each with power in the megawatt range. In order to reach this power requirement, while keeping the ohmic losses in the cavity at a manageable level ($\lesssim 3$ kW/cm^2), emphasis is put on the design and test of overmoded cavities operating close to the minimum quality factor value Q [3]. As a consequence of such an approach, effects of load mismatch could become important as power variations and frequency pulling occur as in any oscillator. Moreover, because the gyrotron open cavity, the transmission line and the load are overmoded and form a whole, reflection can induce oscillations in other longitudinal modes (TE_{mpq}, q=2,3,...) or even in other transverse modes ($TE_{m'p'q'}$). This phenomena is related to the fact that when the Q of the desired oscillating mode approaches its minimum value, neighbouring resonant modes have a comparable Q value and consequently can be easily excited in the presence of reflections. These spurious modes must satisfy the usual requirements for onset of the oscillation : the oscillating frequency is given by $\omega \cong \Omega_c/\gamma \pm k_z v_z$, and the operating beam current must exceed the starting current for the corresponding mode. In our TE^o_{011}, 8 GHz gyrotron oscillator experiment, we have observed the TE^o_{012} longitudinal mode at 8.1 GHz. Depending on the load characteristics, oscillations at 7.1 and 9.3 GHz were also observed. These two frequencies satisfy the above conditions for the TE^o_{211} travelling mode. Similar observations were made on the Thomson CSF TE^o_{511} 8 GHz gyrotron [4].

In this paper we shall concentrate on the pulling and long transmission line effects on the TE^o_{011} mode of our 8 GHz gyrotron [5]. Numerical Rieke diagrams for this gyrotron are presented in Chapter II. Chapter III is devoted to experimental techniques and results. Our measurements confirm the fact that reflections usually lead to a decrease in output power, but for some specific values of the phase and amplitude of the load impedance the output power can exceed the value obtained under matched conditions. We shall discuss the experimental results in Chapter IV.

II. RIEKE DIAGRAM

A. *Rieke Diagram for the Van der Pol Oscillator*

Van der Pol [6] described the simplest oscillator allowing for nonlinearity. The oscillator admittance can be written as a function of angular oscillation frequency ω and circuit voltage amplitude squared $|V|^2$ as :

$$Y(i\omega,|V|^2) = - G_O + G_V|V|^2 + iB_\omega \Delta\omega \qquad (1)$$

where $\Delta\omega=\omega-\omega_O$, and ω_O is the angular oscillation frequency when the circuit is connected to a matched load. By applying Kirchhoff's second law to the oscillator connected to a load of admittance $Y_L=G_L+iB_L$ we have

$$Y(i\omega,|V|^2) + Y_L = 0 \qquad (2)$$

The effect of a mismatched load on the oscillator is to change both its frequency (frequency pulling $\Delta\omega$) and output power (proportional to $|V|^2$)

$$P_{out} = G_L |V|^2 \qquad (3)$$

with respect to the matched condition values.

The Rieke diagram, a plot of equi-frequency and equi-power lines in the complex plane of reflection coefficient (ρ), is a convenient way of representing such effects. Figure 1 shows the Rieke diagram corresponding to the ideal Van der Pol oscillator described by (1) [7].

The main features of this diagram are :

1°) equi-power and equi-frequency lines are circles corresponding to contours of constant resistance and reactance of the Smith chart and thus the diagram is symmetric with respect to the zero admittance line,

2°) the circle of maximum output power passes through the point of zero reflection ($|\rho|=0$).

3°) there is a region where frequency lines converge ("sink") but where no oscillation is possible. Because of overloading the r-f voltage falls to zero.

B. *Rieke Diagram for the Gyrotron Oscillator*

The single mode behaviour of the gyrotron oscillator can be described by the following set of fully relativistic self-consistent equations for γ, the electron relativistic factor, $\Psi=(\omega t-\Phi-(m-1)\theta_g)t$, the slow time scale phase (where $\Phi=(\Omega_c/\gamma)(t-t_o)$ is the particle gyro-phase and θ_g the initial phase), p_z, the longitudinal momentum normalised to m_oc, and $F=(e/2m_oc^2)(E/k)$, the normalised electric field amplitude :

$$\frac{d\gamma}{d\hat{z}} = -\frac{k_\perp}{k} J_{m-1}(k_\perp R_g) \frac{p_\perp}{p_z} \mathrm{Re}\left\{F e^{-i\Psi}\right\} \tag{4}$$

$$\frac{d\Psi}{d\hat{z}} = \frac{\gamma - \Omega_c/\omega}{p_z} - \frac{k_\perp}{k} \frac{J_{m-1}(k_\perp R_g)}{p_\perp p_z} \left[\gamma \mathrm{Im}\left\{F e^{-i\Psi}\right\} + p_z \mathrm{Re}\left\{\frac{dF}{d\hat{z}} e^{-i\Psi}\right\}\right] \tag{5}$$

$$\frac{dp_z}{d\hat{z}} = -\frac{k_\perp}{k} J_{m-1}(k_\perp R_g) \frac{p_\perp}{p_z} \mathrm{Im}\left\{\frac{dF}{d\hat{z}} e^{-i\Psi}\right\} \tag{6}$$

$$\left(\frac{d^2}{d\hat{z}^2} + \left(1-\frac{k_\perp^2}{k^2}\right) - \frac{k_\perp^2}{k^2}(1-i)\frac{\delta}{R}\right) F = i\frac{eZ_oI_b}{m_oc^2} \frac{1}{C_{mp}} \frac{k_\perp}{k} \left\langle J_{m-1}(k_\perp R_g) \frac{p_\perp}{p_z} e^{i\Psi} \right\rangle \tag{7}$$

where $\hat{z}=(\omega/c)z=kz$ is the normalised length, $\Omega_c=(eB/m_o)$ is the cyclotron frequency, $\delta=(2/\omega\mu_o\sigma)^{1/2}$ is the skin depth (with σ the copper conductivity), $C_{mp}=2\pi(\nu^2_{mp}-m^2)J^2_m(\nu_{mp})$ is a normalisation constant for TE^o_{mp} mode at the first harmonic, with $J'_m(\nu_{mp})=0$, R_g is the beam guiding center radius, $R(\hat{z})$ is the cavity radius, Z_o is the vacuum impedance and I_b is the beam current. In eq. (7) the phase average of a quantity f is taken as :

$$\langle f\rangle = \frac{1}{2\pi}\int_0^{2\pi} f\, d\Psi_o \tag{8}$$

$\left.\frac{dE}{dz}\right|_{z=0}=-ik_zE_o$, For given initial conditions (γ_o, p_{zo}, Ψ_o) for the particles and (E_o, ω) for the wave, equations (4) to (7) can be integrated from

the input (z=0) to the output (z=Z) of the cavity. In our model the cavity is followed by an uptaper section of one vacuum wavelength (λ_{vacuum}) and a straight section of the same length. This does not correspond to the experimental conditions where the output waveguide diameter and length are much larger (cf. Chapter IV). The output power :

$$P_{out}=\frac{\pi}{2Z_o}(\nu^2_{mp}-m^2)\,J^2_m(\nu_{mp})\left(\frac{2mc^2}{e}\right)^2\left(\frac{\omega}{\Omega_c}\right)^2 \mathrm{Im}\left\{\frac{1}{F}\frac{dF}{d\hat{z}}\right\}\Bigg|_{z=Z} \qquad (9)$$

and the complex wave impedance ($-E_\theta/H_r$ for a circular TE mode) :

$$Z_{wave} = i\,Z_o\,k\left(\frac{1}{F}\frac{dF}{d\hat{z}}\right)^{-1} \qquad (10)$$

are numerically obtained, and P_{out} and ω are interpreted as the response of the oscillator when submitted to a load of complex reflection coefficient given by

$$\rho = \frac{(Z_{wave}-Z_{waveguide})}{(Z_{wave}+Z_{waveguide})}\Bigg|_{z=Z} \qquad (11)$$

where $Z_{waveguide}$ is the impedance of the corresponding output waveguide mode ($Z_{waveguide}=(k/k_{||})Z_o$). The full diagram is obtained by properly scanning the (ω, E_o) domain. Figures 2(a) & (b) show typical diagrams for the Q_{cav}=225, TE^o_{011} gyrotron [cf.§III.A] at beam currents of 4 and 8 A. The general shape is similar to Fig. 1 but :

1°) the diagram is asymmetric,

2°) the locus of the maximum output power is a single point and is not at $|\rho|=0$ i.e. the maximum output power is achieved only under unmatched conditions,

3°) there is a region where equi-frequency lines converge and where two or more frequencies can be present together, for the same load characteristics, with corresponding powers which can be very different. This region of the diagram will be called the "unstable" region.

III. EXPERIMENT

A. *Gyrotron characteristics*

The design characteristics are given in TABLE 1. Figure 3 shows a good agreement between the experimental results and the numerical values obtained from the non self-consistent computation (using the cold cavity rf profile instead of the self-consistent solution from eq. (7)) for the operating conditions on a matched load. The values of $\alpha=p_\perp/p_z$ derived from the optimum experimental magnetic field profiles have been used for the calculations. The maximum output power ($P_{matched}$) and efficiency under matched conditions are 310 kW (η=35%, I_b=11 A, τ=5 ms) and 43% (I_b=5 A, $P_{matched}$=172 kW). The k-spectrum (Fig. 4) shows a very high mode purity (>99% of TE^o_{011} at 8.018 GHz, I_b=6 A). Note that the k-spectrometer coupling factors for all the modes having a ratio $k_\perp/k_\parallel$ greater than that of the TE^o_{011} are at least 4 dB larger than that of the TE^o_{011}. The measured frequency pulling is of the order of 20 MHz for currents between 1 and 11 A and B-fields between 3.1 and 3.25 kGauss.

B. *Experimental Technique*

The unmatched load consists of a phenolic resin window inserted in the C18 output waveguide and of alcohol which absorbs the transmitted microwave power. Figure 5 shows that this kind of load reflects most of the power in the incident TE^o_{01} mode. The amplitude of the reflection coefficient is changed by varying the window thickness and the phase of the reflected wave by varying the output line length (i.e. the distance between the gyrotron cavity and the load) by a length L ($\Delta\phi=2k_\parallel L$). The output power, the amplitude of the reflection coefficients and the spatial mode content of the reflected signal are measured with a k-spectrometer [8]. In principle, combining the forward and backward signals from the k-spectrometer in an interferometric arrangement would yield the phase of the reflected signal with respect to the incident one. We found that severe cross-talk between the two arms of the k-spectrometer render such a measurement impossible. The pulse frequency stability and content are checked via a frequency discriminator and the precise frequency value is measured with a spectrum analyser. At each beam current, the magnetic field is set to optimise the output power delivered to a matched "cone calorimeter" (VSWR=1.4:1, $|\rho_{power}|$=3%).

Under these matched conditions, the output power ($P_{matched}$) was 130 kW at 8.015 GHz and I_b=4 A. Figures 6(a) through (d) show the output power and frequency pulling versus $\Delta\phi$ at I_b=4 A for power reflection coefficients ($|\rho_{power}|$) from 9.5% up to 40% (VSWR=1.89:1 to 4.51:1). TABLE 2 gives a comparison between the experiment and the numerical predictions for the output power variations, and frequency pulling over a 2π phase rotation for four VSWR values. With the VSWR=4.51:1, two pulses out of three were cut by the H.V. modulator due to internal tube arcing. However, after such an arc, the gyrotron did not need to be reconditioned and could immediately withstand the full beam voltage and current when again used with a matched load.

The same experiment was repeated at I_b=6 A ($P_{matched}$=180 kW at 8.018 GHz). A VSWR=1.89:1 already led to arcing and to mode switching to the TE^{o}_{012} at 8.108 GHz. At higher currents, operation was possible only with the calorimeter, i.e. under a VSWR of 1.4:1.

IV. DISCUSSION

When increasing the reflection coefficient at a beam current of 4 A, the average output power decreases for all the 8 values of $k_{||}L$. Nevertheless, Figures 6(a) & (b) show that power reflection can lead to an output power up to 15% greater than under matched conditions, as predicted by the numerical Rieke diagram. Figures 6 are periodic with a period of $2k_{||}L=2\pi$. Except for jumps from the minimum to the maximum of the frequency pulling, only a monotonic frequency decrease was observed when moving the load away from the gyrotron cavity. Maximum output power always occurs for values of $2k_{||}L$ close to the one corresponding to the frequency jump. This jump together with the corresponding power variation were observed when going from one such value of line length to the other or even sometimes during a single pulse. Rieke diagrams (Fig. 2(a)a& (b) indicate that this behaviour should occur when approaching the "unstable" region. This region is characterized by a high sensitivity of the output power and oscillation frequency to the load characteristics.

The maximum measured frequency pulling is ±7 MHz (cf. TABLE 2) although the calculated value is larger (±21 MHz). An explanation of this discrepancy can be provided by considering the actual transmission line which follows the gyrotron cavity and which is formed by the collector, the k-spectrometer and the load. These components have their own reflection coefficient and thus form an external cavity with its own mode structure and quality factor Q_{ext}. Calculations (Rieke diagrams Fig. 2.(a) & (b) only take into account a line length $L\cong 2\lambda_{vacuum}$. Using the actual value of the total 4 meters ($L\cong 100\lambda_{vacuum}$) C18 line one finds that the resonant frequencies of the longitudinal line modes are separated by Δf

$$\Delta f = \frac{c}{2L} = 37.5 \text{ MHz} \qquad (12)$$

and an estimation of the quality factor is given by [9,10]

$$Q_{ext} = - \frac{\omega k L}{\ln|\rho_{ampl.}|\, k_{||} c} \qquad (13)$$

which leads to Q values between 600 and 1500 for amplitude reflection coefficient $|\rho_{ampl.}|$ from 0.33 to 0.63 (VSWR 1.89:1 to 4.51:1) and correspond to FWHM of 13 to 5 MHz.

As observed in other experiments [11,12] this external cavity imposes its own passband stopband structure on the gyrotron. The calculations presented in paragraph II.B apply to the case where the external Q is much smaller than the cavity Q ($Q_{ext} \sim L = 2\lambda_{vacuum} << Q_{cav}$). Under such short line condition, the frequency pulling (±21 MHz for $VSWR_{max}$=4.51:1) is an intrinsic property of the gyrotron cavity rather than a property of the system formed by the cavity plus the transmission line. Since in the experiment $Q_{ext} >> Q_{cav}$ the measured frequency pulling is determined by the line which follows the cavity. Mode hopping by Δf=37.5 MHz did not occur since Δf is comparable to the maximum frequency pulling under short line conditions. The oscillation is locked into one external mode and we do not observe the band structure [11,12]. This explains the discrepancy between the calculated and measured frequency pulling values in TABLE 2, and also the fact that the "unstable" region is not seen, as it should occur at frequencies which are out of the $f_{matched} \pm 7$ MHz passband. When the phase of the reflection reaches the passband limit, the oscillation characteristics jump from one band limit to the other.

In our low order TE^{o}_{011} mode cavity, competition can occur with parasitic longitudinal modes (TE^{o}_{01q}, q=2,3,...). When going to low Q, their quality factors become closer and closer ($Q_{cav}=Q(TE^{o}_{011})$=225 at 8.005 GHz, $Q(TE^{o}_{012})$=180 at 8.095 GHz for this cavity). At I_b=6 A, a 9.5% power reflection (VSWR=1.89:1) was sufficient to favour the TE^{o}_{012} mode. It is possible, in principle, to operate on the right mode by tuning the magnetic field ($\Omega_c/\omega \cong \gamma$), even in the presence of reflections.

We were not able to locate where arcing occurs as a result of too high a reflection. Calculations show that very high electric field values are reached inside the cavity (a maximum of 4 MV/m with VSWR=4.51:1), but these values are still well below the conservative Kilpatrick limit [13] (75 MV/m at 8 GHz). If the load converts some fraction of the incident power from TE^{o}_{01} to TE^{o}_{11}, this mode could then reach the drift region between the gun and the cavity which is not at cut-off for the TE^{o}_{11} mode. Beam disturbance in this region where the beam is close to the wall could cause beam interception and pulse switching-off by the H.V. modulator.

V. CONCLUSION

We have demonstrated stable operation under matched condition of a 8 GHz low Q (225) gyrotron up to a power of 310 kW with an efficiency of 35% and a 5 ms pulse length. We have investigated the effect of power reflections on the tube behaviour. At low power (I_b=4 A, $P_{matched}$=130 kW) the oscillator could stand reflections up to $|\rho_{power}|$=40% , resulting mainly in power reduction, and finally in internal arcing. Nevertheless, we found some reflection coefficient values (phase and amplitude) leading to powers up to 150 kW. The sensitivity to reflections dramatically increases with output power and beam current, and at full power (310 kW) operation is only possible on a load with a VSWR $\leq$1.4:1. The measured frequency pulling is smaller than the computed one. We attribute this to the influence of the long transmission line which imposes its own mode spectrum to gyrotron.

ACKNOWLEDGEMENT

This work was partially supported by the "Commission pour l'Encouragement de la Recherche Scientifique", Grant N° 1773.1., by the "Fonds National Suisse de la Recherche Scientifique", and by the internal R and D program of the EKR Department of ABB INFOCOM SA. We would like to thank Dr. G. Mourier for discussions on parasitic oscillations.

Cold cavity characteristics	
Mode	TE^{o}_{011}
Diffractive Q (Q_{cav})	225
Resonant frequency (GHz)	8.005
Mode	TE^{o}_{012}
Diffractive Q	180
Resonant frequency (GHz)	8.095
Beam parameters	
Cathode voltage (kV)	80
Beam current (A)	10
$\alpha=p_{\perp}/p_z$	1.89
Magnetic field (kGauss)	3.20
Average beam radius (cm)	1.15
Beam thickness (cm)	0.4
Cathode	
Current density (A/cm^2)	1.5

TABLE 1 : Gyrotron design parameters.

[11] "Frequency pulling and bandwidth measurements of 140 GHz pulsed gyrotron", K. E. Kreischer, B. G. Dandly, P. Woskoboinikow, W. J. Mulligan and R. J. Temkin, *Int. J. Electronics.*, vol. 57, pp. 851-862, 1984.

[12] "Accurate frequency measurement on gyrotrons using a 'gyro-radiometer'", L. Rebuffi, EUR-CEA-FC-1306, August 1986.

[13] "Criterion for vacuum sparking designed to include both rf and dc" W. D. Kilpatrick, *Rev. Sci. Instrum.*, vol. 28, 824 (1957).

REFERENCES

[1] "A high power gyrotron oscillator at 8 GHz", H.-G. Mathews, G. Agosti, K. Holm, D. Kuse, P. Muggli, M. Q. Tran, T. M. Tran, S. Alberti and A. Perrenoud, *Proc. of 12th Conference on Infrared and Millimeter Waves,* Florida, pp. 383-384, 1987.

[2] "The design of megawatt gyrotrons for the Compact Ignition Tokamak", K. E. Kreischer, T. L. Grimm, A. W. Mobius and R. J. Temkin, *Proc. of 13th Conference on Infrared and Millimeter Waves,* Hawaii, pp. 179-180, 1988.

[3] "Theory of gyrotron with a nonfixed structure of the high-frequency field", V. L. Bratman, M. A. Moiseev, M. I. Petelin and R. E. Erm, *Radiophys. Quantum Electron.*, vol. 16, 474 (1973).

[4] G. Mourier, private communication.

[5] "Effect of power reflection on the operation of a low Q, 8 GHz gyrotron", P. Muggli, M. Q. Tran, T. M. Tran, H.-G. Mathews, G. Agosti, S. Alberti and A. Perrenoud, *Bulletin of the American Physical Society*, vol. 33, N° 9, October 1988.

[6] "Forced oscillations in a circuit with non-linear resistance", B. van der Pol, *Phil. Mag*, S. 7, vol. 3, N° 13, Jan. 1927.

[7] "Locking phenomena in microwave oscillator circuits", M. Nakajima, and J, Ikenoue, *Int. J. Electronics.*, vol. 44, pp 465-472, 1978.

[8] "A novel device for multimedia analysis in oversized waveguides", W. Kasparek, G.A. Müller, *Proc. of 10th Conference on Infrared and Millimeter Waves,* Florida, pp. 238-239, 1985.

[9] "Irregular waveguides as open resonators", S. N. Vlasov, G. M. Zhislin, I. M. Orlova, M. I. Petelin, and G. G. Rogacheva, *Radiophys. Quantum Elect.*, vol. 12, pp. 972-978, 1969.

[10] "Analytic theory of tapered gyrotron resonators", R. J. Temkin, *Int. J. Inf. and Mm .Waves*, vol. 2, pp 629-650, 1981.

VSWR	Power variations (kW)		Freq. pulling (MHz)		Minimum Power (kW)
	calc.	exp.	calc.	exp.	exp.
1.89:1	10	29	±14	±6	106
2.65:1	30	24	±16	±7	104
3.21:1	50	63	±18	±7	86
4.51:1	70	37	±21	±7	89

TABLE 2 : Comparison between the calculations and the experiment for the output power variation (maximum amplitude) and maximum frequency pulling over a $2k_{||}L = 2\pi$ phase rotation for the four VSWR values. The last column gives the minimum power measured over a 2π phase variation.

Figure captions

Fig. 1 : Rieke diagram for an ideal van der Pol oscillator described by the output admittance given by (1). Equi-power and equi-frequency lines are circles corresponding to contours of constant resistance and reactance of the Smith chart and the diagram is symmetric. There is a region where all frequency lines converge ("sink" region) where no oscillation is possible due to voltage overload. The circle of maximum output power passes through the point of zero reflection ($|\rho|=0$). The output power ($\bar{P}$) is normalised to its maximum value and the frequency pulling ($\Delta\omega=\omega-\omega_o$) is defined with respect to the oscillation frequency under matched condition (ω_o).

Fig. 2 : Rieke diagrams for a gyrotron having a cavity cold Q of 225 (TE^o_{011}). The cathode voltage is 80 kV.

a. For this figure the parameters are: I_b=4 A, B-field=3.20 kGauss, $\alpha=p_\perp/p_z$=1.75 (experimental value). The characteristics under matched conditions are: f=8.003 GHz (the frequency curves are labelled with respect to this value) and $P_{matched}$=160 kW. The unstable region is very close to the $|\rho|=0$ point because the chosen B-field value is very close to the starting current.

b. For this figure the parameters are: I_b=8 A, B-field=3.21 kGauss, α=1.40 (experimental value). The characteristics under matched conditions are: f=8.018 GHz (the frequency curves are labelled with respect to this value) and $P_{matched}$=235 kW.

Fig. 3 : Comparison between the measured optimised output power (•) and the non self-consistent calculation (Δ). The value of α (□) found through the experimental B-field profile is shown and is used for the calculations.

Fig. 4 : K-spectrum at I_b=6 A, B-field=3.143 kGauss and f=8.018 GHz with the cone calorimeter as load (i.e. matched condition VSWR=1.4:1). This spectrum shows a very high TE^o_{011} mode purity. The TE^o_{01} signal appears at an angle of 23° with the

$\vec{E} \perp \vec{k}$ polarisation (the $\vec{E} \parallel \vec{k}$ showed no signal and is not plotted). Note that the computed coupling coefficients for the TE^{o}_{01} mode is at least 4 dB lower than for other TE^{o}_{mp} modes having a greater ratio $k_{\perp}/k_{\parallel}$.

Fig. 5 : K-spectrum at I_b=4 A, B-field=3.12 kGauss and f=8.011 GHz for the VSWR=3.21:1 load. This spectrum shows that most of the power is reflected in the incident TE^{o}_{01} mode (the line corresponds to the $\vec{E} \perp \vec{k}$ polarisation, the $\vec{E} \parallel \vec{k}$ showed no signal and is not plotted)

Fig. 6 : Output power and frequency pulling vs. $2k_{\parallel}L$ at I_b=4 A, B-field=3.12 kGauss for four values of power reflection:

a. $|\rho_{power}|$= 9.5% (VSWR=1.89:1)
b. $|\rho_{power}|$=20.5% (VSWR=2.65:1)
c. $|\rho_{power}|$=28.0% (VSWR=3.21:1)
d. $|\rho_{power}|$=40.0% (VSWR=4.51:1)

The optimum output power under matched condition was 130 kW (indicated by the straight line) at 8.015 GHz. Figures (a) & (c) show that power reflection from the load can lead to output power greater than under matched conditions.

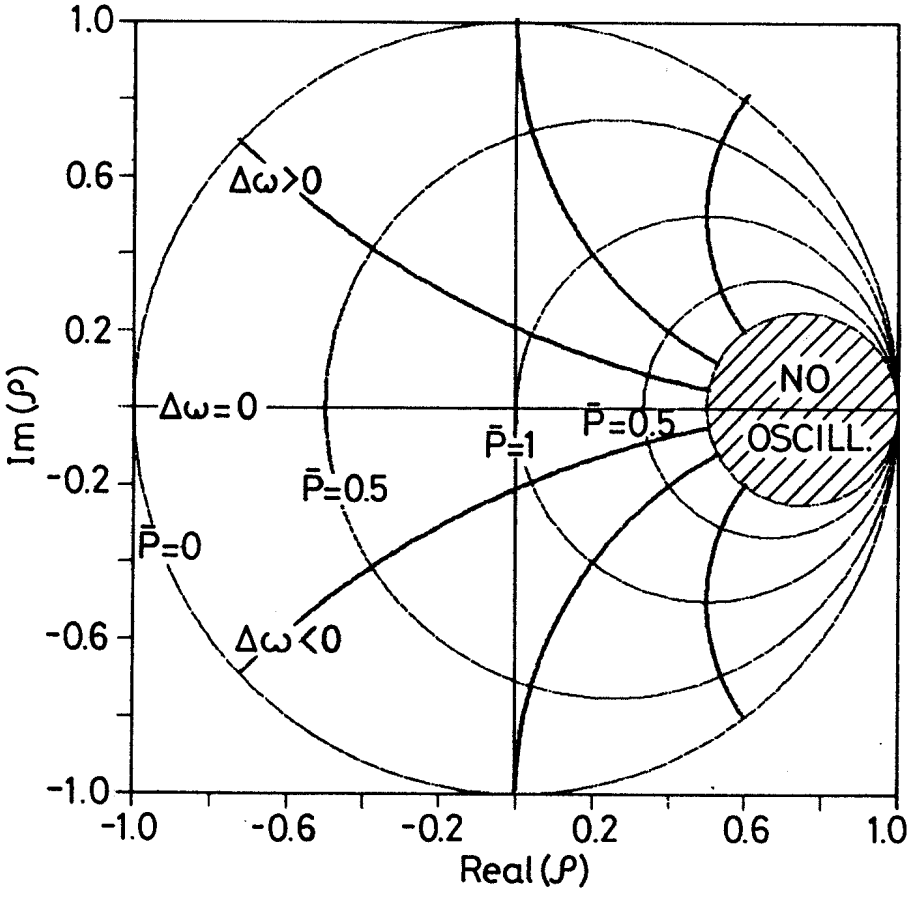
1.0
0.6
0.2
-0.2
-0.6
-1.0
-1.0
-0.6
-0.2
0.2
0.6
1.0
Im (ρ)
Real (ρ)
Δω>0
Δω=0
Δω<0
P̄=0
P̄=0.5
P̄=1
P̄=0.5
NO
OSCILL.

FIG. 1

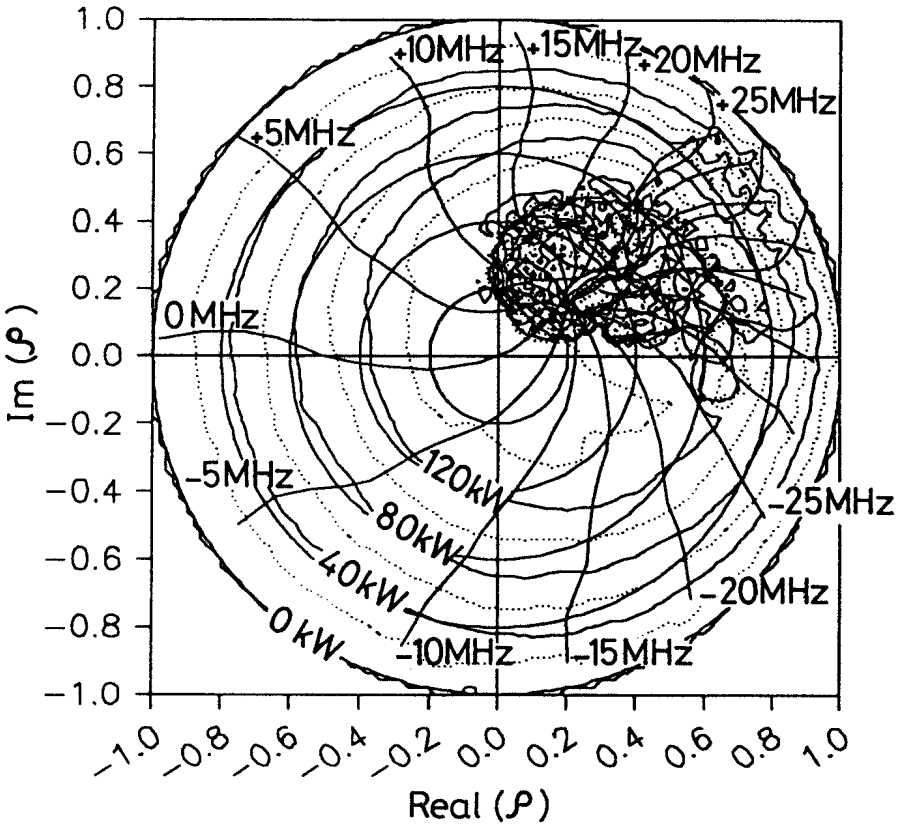
1.0
0.8
0.6
0.4
0.2
0.0
−0.2
−0.4
−0.6
−0.8
−1.0
Im (ρ)
+10MHz
+15MHz
+20MHz
+25MHz
+5MHz
0MHz
-5MHz
120kW
80kW
40kW
0kW
-10MHz
-15MHz
-20MHz
-25MHz
−1.0
−0.8
−0.6
−0.4
−0.2
0.0
0.2
0.4
0.6
0.8
1.0
Real (ρ)

FIG. 2(A)

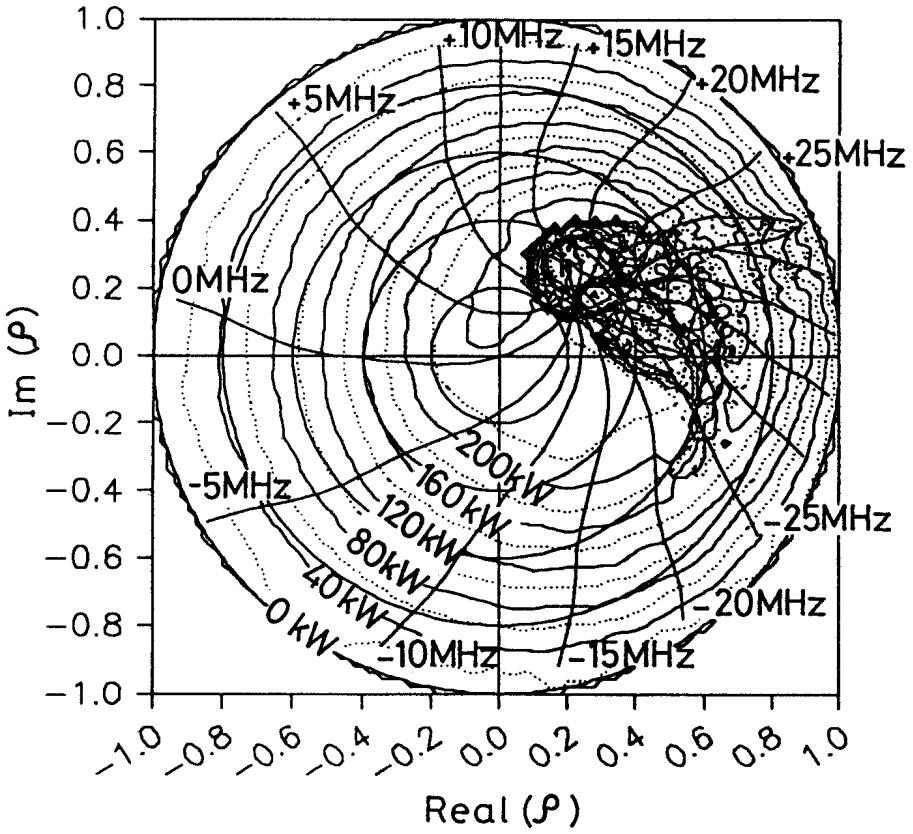
1.0
0.8
0.6
0.4
0.2
0.0
−0.2
−0.4
−0.6
−0.8
−1.0
Im (ρ)
−1.0 −0.8 −0.6 −0.4 −0.2 0.0 0.2 0.4 0.6 0.8 1.0
Real (ρ)
+10MHz
+15MHz
+20MHz
+25MHz
+5MHz
0MHz
-5MHz
-25MHz
-20MHz
-15MHz
-10MHz
200kW
160kW
120kW
80kW
40kW
0 kW

FIG. 2(B)

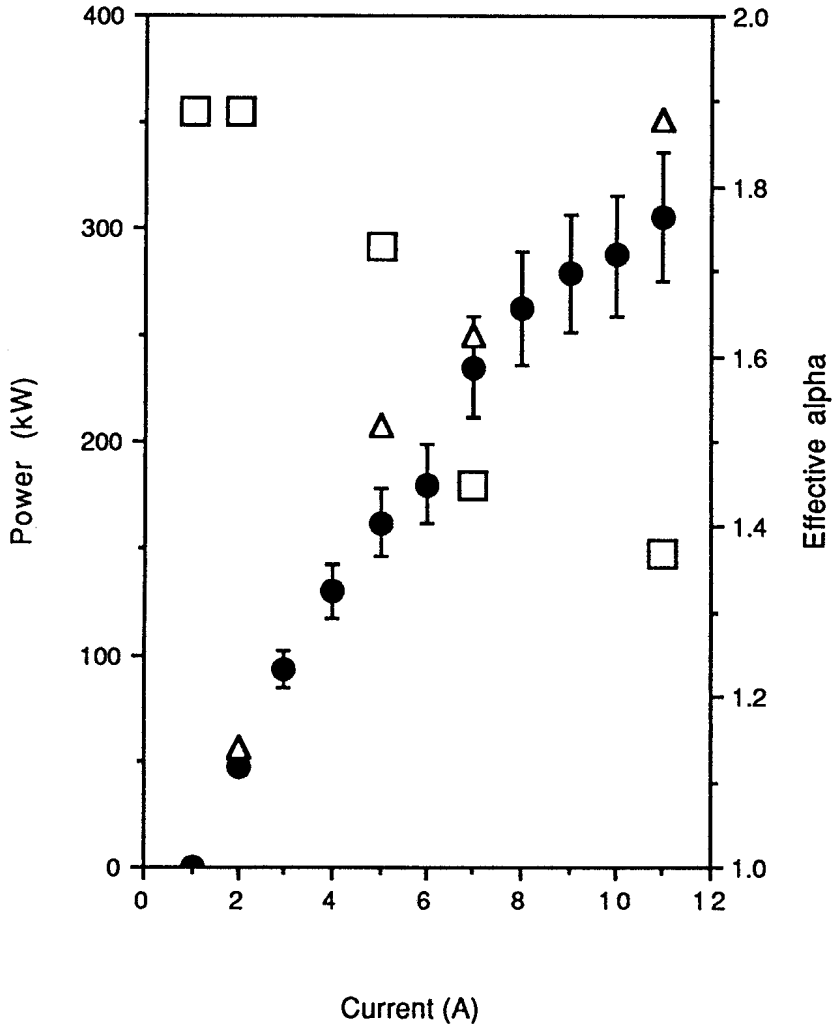
400
300
200
100
0
2.0
1.8
1.6
1.4
1.2
1.0
0
2
4
6
8
10
12
Power (kW)
Effective alpha
Current (A)

FIG. 3

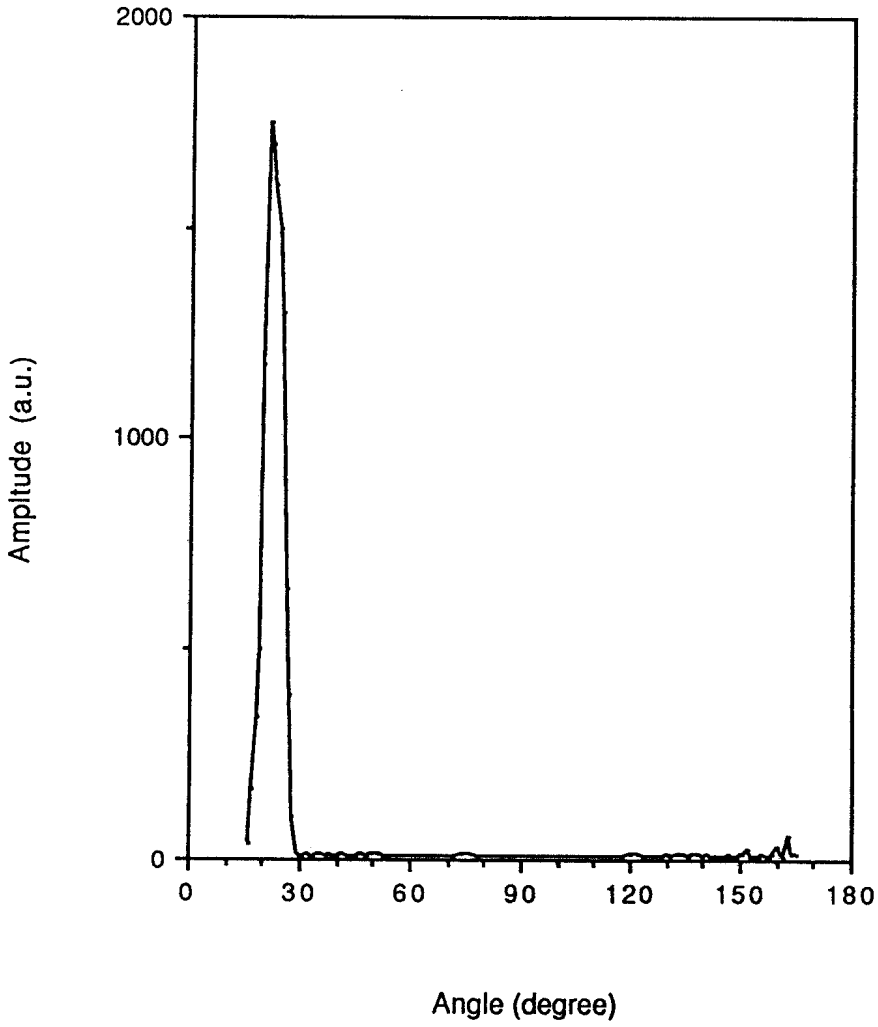

FIG. 4

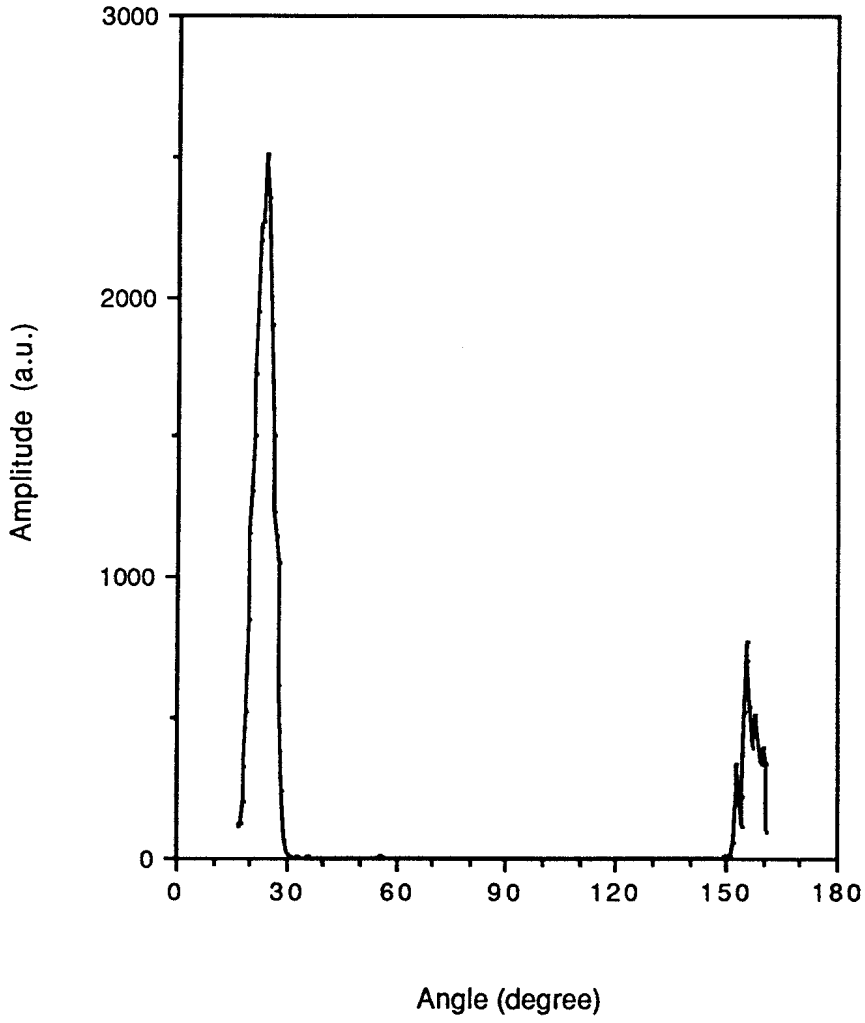
3000
2000
1000
0
Amplitude (a.u.)
0
30
60
90
120
150
180
Angle (degree)

FIG. 5

Fig.5.a. VSWR=1.89:1

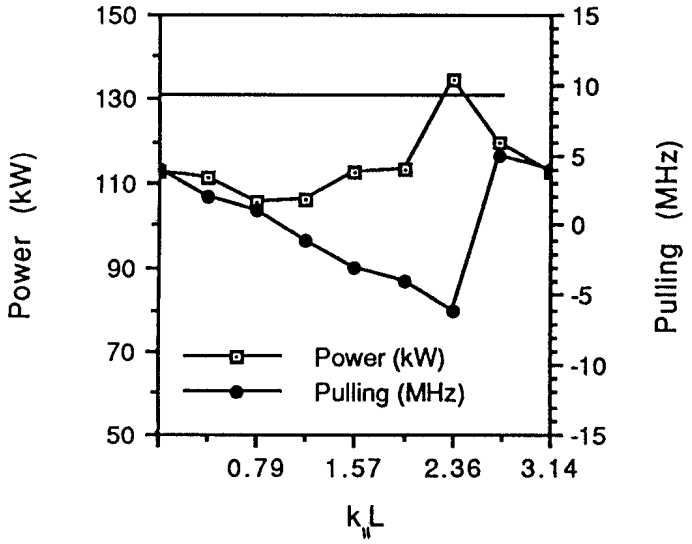

Fig.5.b. VSWR=2.65:1

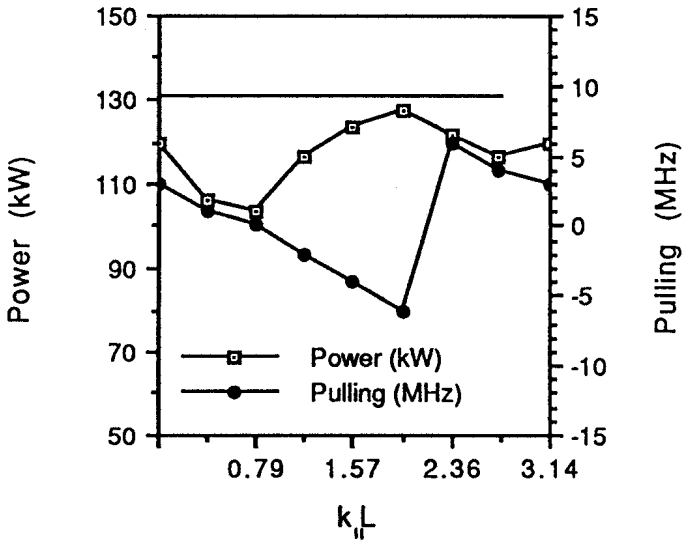

Fig.5.c. VSWR=3.21:1

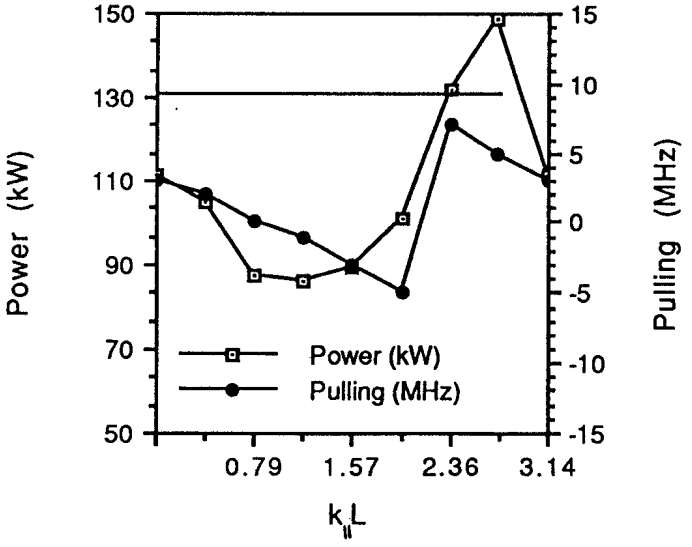

Fig.5.d. VSWR=4.51:1

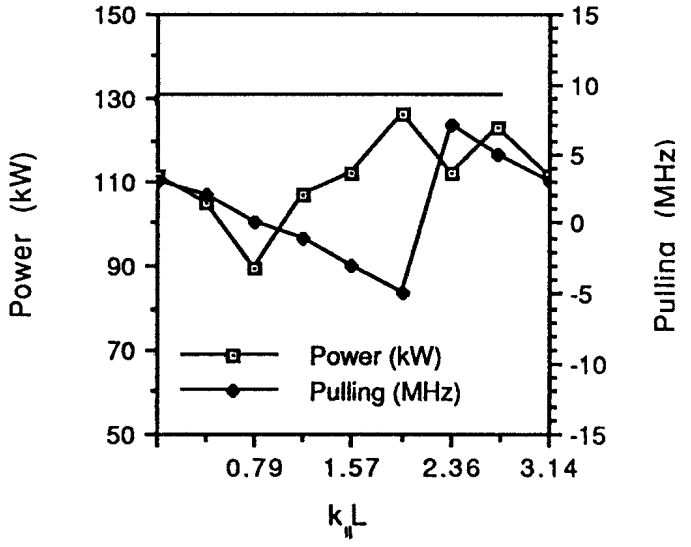

FIG. 6